Investigation and Application of Nanoparticle Dispersions of Pigment Yellow 185 using Organic Solvents

Algernon T. Kelley,[†] Paula J. Alessi,[‡] Jill E. Fornalik,[‡] John R. Minter,[‡] Peter G. Bessey,[‡] Jayne C. Garno,[†] and Tommie L. Royster, Jr.*[,‡]

Department of Chemistry, Louisiana State University, Baton Rouge, Louisiana 70803, and Eastman Kodak Company, Research Laboratory, Rochester, New York 14650

ABSTRACT Self-aggregation of organic pigment nanoparticles in organic solvent produces poor quality thin-film coatings. The nonuniformity of surface layers produced by dense aggregates within films of nanopigments can be detrimental for light transmission. Formulating dispersions composed of an organic pigment and an organic solvent with minimized aggregation must be achieved for use as precursors for high-performance optical thin-films. The goal of our investigation was to determine the influence of deaggregating dispersants with and without a surface-modifying synergist, as well as the influence of solvent polarity on the dispersion properties. The work was focused on establishing nanoparticles smaller than 50 nm in size, which is an area not broadly published for solvent-based systems. A working hypothesis of using an acid-functionalized synergist capable of establishing stable acid/base ionic-pair interactions was investigated. Our work demonstrated that a synergist that incorporates acid functional groups can be combined with an amine-functionalized polymeric dispersant to form a stable organic solvent-based dispersion composed of dispersed pigment nanoparticles that also incorporate amine functional groups. Stabilizing ionic-pair interactions are proposed. The dispersion and coatings of the dispersion were characterized using dynamic light scattering (DLS), transmission electron microscopy (TEM), and atomic force microscopy (AFM). Optical properties of thin-films were evaluated from transmission spectroscopy measurements. Within this study, a correlation was established between spectral properties of coated dispersions and detected nanoparticle aggregation.

KEYWORDS: atomic force microscopy • organic pigment nanoparticles • dispersion • synergist • dynamic light scattering • transmittance • thin films • PY-185

INTRODUCTION

Pigment nanoparticles or nanopigments are emerging as practical nanomaterials with properties that are intermediate between molecular and bulk materials (1−4). Increasingly, dispersions of organic and inorganic nanopigments are being applied as inks used in digital printing, colorants for paints or coatings, cosmetics, and color filter arrays for the display industry (5−15). The advantages of pigment nanoparticles are based upon properties that provide higher optical densities, an increased range of color scales, and sharper spectral features compared to pigments composed of microparticles (3, 5, 11, 16−18). Additionally, higher transmittance can be achieved for display applications (5, 18, 19).

For several of the applications, pigment nanoparticles are initially formulated into dispersions. Aqueous systems are predominantly used for dispersions that incorporate organic pigments including applications such as inkjet printing (1, 7, 17, 20, 21). Eco-friendly solvent-based systems are also beginning to emerge and are more suitable for certain applications (22). However, dispersing organic pigment nanoparticles that are 50 nm and smaller in organic solvents presents a challenge. Interactions between organic pigments and organic solvents (e.g., hydrogen bonding) can disrupt the interactions with stabilizing dispersants. As a result, significant nanoparticle aggregation that compromises optical properties occur (19). This problem is magnified for dispersions with pigment concentrations in the 10−15% range resulting in high viscosity dispersions. Polymeric dispersants are typically required for good dispersion properties including reduced viscosity (17, 21, 23). Polymer-grafted organic pigments have been reported to produce stable organic solvent-based dispersions (24). However, there are few studies reported that show how dispersants and surface modifying synergists can be used to disperse organic pigment nanoparticles smaller than 50 nm for nonaqueous systems.

Dispersions composed of organic pigment nanoparticles in organic solvent have been produced by methods such as mechanical milling (25) and supercritical antisolvent processes (SAS) (11, 19). Mechanical milling is the most common method used to produce pigment nanoparticles in organic media. This process often involves use of ceramic milling media for particle size reduction (25). Organic pigment dispersions prepared from supercritical antisolvent processes have been carried out in the presence of various aprotic or protic organic solvents (11, 19). Typically, a fluid

* Corresponding author. Phone: (585) 722-5928. E-mail: tommie.royster@kodak.com.

Received for review August 27, 2009 and accepted December 11, 2009

[†] Louisiana State University.

[‡] Eastman Kodak Company.

DOI: 10.1021/am9005836

is termed supercritical when the pressure and temperature are in a state above the fluid critical temperature and pressure, thereby permitting the gaseous and liquid phases to coexist (19, 26). A new dry milling process used for organic pigments in the presence of silica nanoparticles produced uniform hybrid core−shell nanostructures (27, 28). However, attempts to disperse the dry milled nanoparticles in PGMEA resulted in slight aggregation, as determined by DLS measurements combined with TEM images (27).

For pure organic pigments, the resulting particle size achieved using traditional mechanical milling depends upon several variables including the type and size of the milling media, milling speed, dispersant, and solvent type. The typical size range for particles and/or aggregates produced by traditional mechanical milling is 200 nm to 1 μm. The supercritical fluid (CO_2) process produced nanoparticles that ranged from 15 μm to 100 nm (11, 19). This broad range of organic pigment nanoparticles can be attributed to a host of factors including solvent effects, flow rate, temperature, and pressure. The dry milling of organic pigments with silica nanoparticles produced core−shell nanostructures with an average size comparable to the parent silica nanoparticles (~20 nm) as determined by TEM.

To broaden the potential capabilities and applications for nonaqueous dispersions, more fundamental studies in this area are required. Therefore, our work has focused on investigating the role synergist/dispersant interactions can play in forming and dispersing a uniform distribution of nanoparticles smaller than 50 nm in an eco-friendly solvent system. Comprehensive studies that cover the desired particle size distribution for organic pigments dispersed in organic solvents have been difficult to identify. Our studies probe the influences of common polymeric dispersants with known functionality that can potentially react with functional groups on a surface-modifying agent to promote favorable stabilizing interactions. Investigations of the influence of nanoparticle aggregation on resulting spectral properties of thin-films fabricated from the solvent-based dispersions were also carried out. Studies and improvements in this area ultimately can contribute to advancements in the optical performance of thin films made from pigment nanoparticles for commercial applications (29−31).

EXPERIMENTAL SECTION

Materials and Reagents. Commercially available dispersants were used without further purification: Solsperse 22000 from Lubrizol Additives (Wickliffe, Ohio); pigment yellow 185 (PY-185) from BASF Corporation (Florham Park, NJ); and Disperbyk-161 from BYK USA Inc. (Wallingford, CT). Propylene glycol monomethyl ether acetate (PGMEA) and cyclohexanone were obtained from Sigma Aldrich (Milwaukee, WI). The milling media was procured from Eastman Kodak Company.

Preparation of Pigment Yellow 185 Dispersions. In a typical process, 200 g of dispersion was prepared by combining PGMEA with the dispersant polymer Disperbyk 161 in a cold water-jacketed vessel. Then, PY-185 was introduced, followed by 50 μm polystyrene milling media (200 g). The final mixture was composed of 80% PGMEA, 2% butyl acetate,12% PY-185, and 6% active polymer. After milling, the dispersion was isolated by vacuum filtering through 5 μm filter media. For stability evaluation, dispersions were stored in polyethylene bottles at room temperature. Each bottle was agitated before sampling for analysis.

Viscosity Measurements. A coquette geometry vessel was charged with approximately 15 mL of dispersion and placed in an ARES I rheometer. Viscosity measurements were then carried out using a steady shear rate sweep ($1-1000\ sec^{-1}$).

Dynamic Light Scattering (DLS). Samples for particle size distributions of pigment nanoparticles were prepared by diluting approximately 0.5 mL of the dispersion with 3 mL of PGMEA and transferring to a scintillation vial. An additional 6 mL of solvent was added before placing in a sonication bath for 5 s. The sample was then analyzed with a Nanotrac model 150 instrument, previously known as Ultrafine Particle Analyzer (UPA) from Microtrac (Saint-Petersburg, Russia).

Sample Preparation by Spin-Coating. Dispersions were spin-coated on clean glass slides within 48 h of preparation. The substrates used were borosilicate glass 1.1 mm thickness (2.5 × 2.5 μm^2). Glass cleaning was an automated process performed in a class-100 clean room. Slides were cleaned by rinsing with deionized water and then washed for 30 s in a solution of deionized water with Valtron SP 2500 alkaline detergent solution (Valtech Corp., Pottstown, PA). The glass surfaces were rinsed with deionized water and the cycle was repeated once. After rinsing, the slides were dried under nitrogen for 25 s and exposed to an infrared lamp for 25 s. The glass was then spun at 2500 rpm, followed by a spin dry cycle at 2500 rpm for 25 s. The glass plates were transferred to a vacuum-operated spin-coater before placing ~1 mL of the dispersion onto the plate. The sample was spun for 3 s at 100−500 rpm before the speed was ramped to 2500 rpm for 30 s. The coated plate was then air-dried and cured on a hot plate by heating for up to 40 min at 55 °C. The samples were stored for up to 2 months for AFM characterization and optical measurements.

Total Transmittance Measurements. Spectrophotometry measurements of dispersion coated glass plates were made using a CARY 5E UV−vis-NIR Spectrometer from Varian (Palo Alto, CA) with an integrating sphere attachment, operating in total transmittance mode. The total transmittance mode measures both the diffuse and specular components of the sample. Blank substrates of uncoated glass slides were used for a baseline measurement. The blank slides were subjected to the same cleaning procedure as the coated surfaces.

Transmission Electron Microscopy (TEM). Five drops of dispersion were diluted with approximately 5 mL of PGMEA and vortex mixed to homogenize. A single drop of this diluted dispersion was gently placed on the surface of an ultrathin amorphous carbon film supported by a 400 mesh Cu grid (Ted Pella #01822-F). While viewing the drop with a stereo- microscope, a small wedge of filter paper was used to blot away most of the liquid until only a thin liquid film remained coating the surface of the support film. This thin film was permitted to dry onto the support.

After drying overnight, each sample was imaged in a FEI CM20T transmission electron microscope with an accelerating voltage of 200 kV. Images were recorded on a Gatan Ultrascan 1000 CCD camera. Images were recorded with a defocus of approximately −0.5 μm to enhance the phase contrast. Diffraction contrast from the crystalline particles is observed in low-magnification images and disappears during imaging at high magnification as the crystallinity is destroyed by radiation damage, but the particle outlines undergo minimal changes.

Atomic Force Microscopy (AFM). Atomic force microscopy images of dispersion coated glass plates were acquired using a Dimension 3100 scanning probe microscope with maximum scan area of 90 × 90 μm^2 (Veeco Metrology Inc., Santa Barbara, CA). Nanoscope v5.12 software was used for data acquisition. Digital images were processed with Gwyddion (version 2.9),

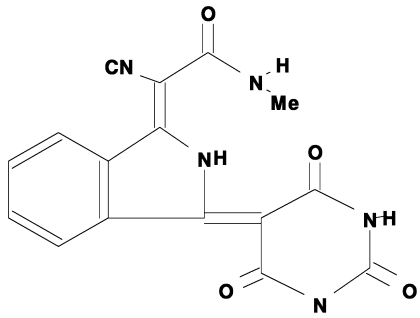

FIGURE 1. Molecular structure of PY-185.

which is open source software supported by the Czech Metrology Institute freely available on the Internet (http://gwyddion.net). Commercially available silicon nitride cantilevers with resonance frequencies ranging from 200 to 400 kHz, and spring constants ranging from 20 to 80 N/m were used for imaging in tapping mode (Veeco Probes, Santa Barbara, CA).

RESULTS AND DISCUSSION

Before investigating the capability of blocking aggregation of nanoparticles smaller than 50 nm, a process was needed to generate a uniform distribution of nanoparticles in the desired particle size range. To accomplish this goal, pigment yellow 185 (PY-185) was combined with dispersing polymers in PGMEA and then mechanically milled using polystyrene milling media developed at Eastman Kodak Company. The molecular structure of PY-185 shown in Figure 1 incorporates three amine functional groups. Therefore, dispersing polymers with amine functional groups were targeted for evaluation.

It was determined that the amine-based dispersant Disperbyk - 161 worked very effectively for generating and dispersing PY-185 nanoparticles while maintaining a low viscosity. The quoted amine value (0.2 mequiv/g) was confirmed experimentally using a titration method. The objective was to determine if favorable amine-to-amine interactions (including hydrogen bonding) between the surface of pigment nanoparticles and the polymeric dispersant were sufficient to promote the formation and stabilize dispersed nanoparticles.

Dynamic light scattering (DLS) measurements were used to assess the particle size distribution and stability of the resulting dispersions. Particle sizing data were collected within 24 h and after 90 days of preparation. Size distribution plots of the reference dispersion, composed of PY-185, PGMEA, and Disperbyk-161, are represented in Figure 2. Each plot showed a dominant population of nanoparticles in the 10−50 nm range. A second population above 100 nm was also observed. The plot acquired after 90 days showed a detectable shift toward larger particles, indicating instability from possible particle aggregation.

The apparent dispersion instability and aggregation could result from relatively weak amine- to-amine interactions between the dispersant and pigment nanoparticles. Researchers have shown that synergist compounds can be used to promote interactions between polymeric dispersants and the surface of pigment particles for nonaqueous dispersions (32). As a result, these compounds have also been

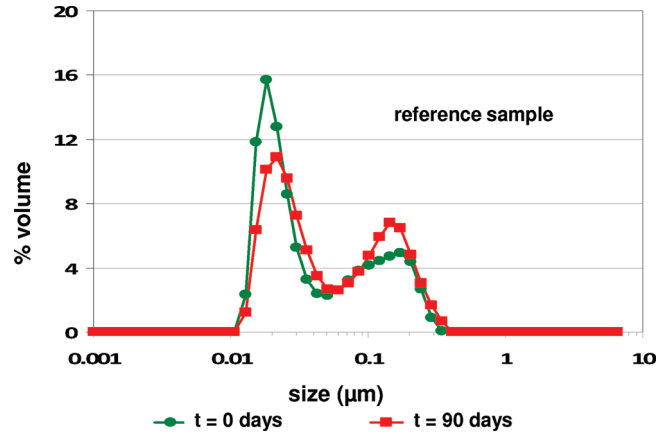

FIGURE 2. Size analysis (DLS) of reference pigment nanoparticles prepared in PGMEA. Analyses were carried out immediately after dispersion preparation and after aging for 3 months.

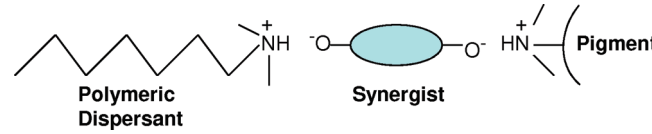

FIGURE 3. Diagram of proposed acid/base ion-pair interactions between dispersant polymer, synergist, and pigment nanoparticle.

noted for reduction in particle aggregation. Some synergist compounds incorporate acidic functional groups such as sulfonic and carboxylic acid groups (32). Acid functionalized synergists were of interest for elucidating if acid/base reactions involving amine functional groups of Disperbyk 161 and PY-185 would result in a stable link between the polymeric dispersant and the surface of generated PY-185 nanoparticles. The link would result from formation of acid/base ion-pair interactions. The proposed interactions are illustrated in Figure 3. In theory, these surface interactions would result in the formation of nanomicelles with the polymeric chain interacting with the solvent, PGMEA (possibly through detected ester groups).

The synergist Solsperse 22000, a yellow proprietary pigment with acid functionality was chosen for the study to probe the influence of PY-185 surface modification. The synergist was introduced under the same dispersion preparation conditions as the reference dispersion. A very low viscosity was indicated from steady shear rate sweep measurements producing an average viscosity of 5.2 cps. Size distributions acquired with DLS of the resulting dispersions are represented in Figure 4. The plots show a more uniform size distribution compared to the reference control sample in Figure 2 with a mean nanoparticle size of 12 nm. There was no significant detection (2.2%) of particles larger than 100 nm. In addition, no detectable shift in the size distribution was observed after 90 days, indicating improved stability for the dispersion formulation. These data indicate the detection of particles above 100 nm and the instability observed for the reference dispersion could result from nanoparticle aggregation.

Characterization of pigment nanoparticles using TEM was carried out to confirm nanoparticle formation and to determine if there is a detectable particle size difference between

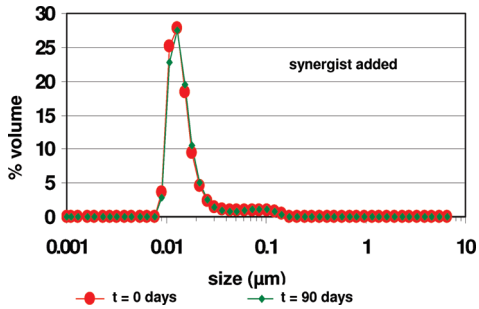

FIGURE 4. Size distribution of pigment nanoparticles in PGME with synergist obtained by DLS. Analyses were carried out immediately after preparing dispersions and after 3 months.

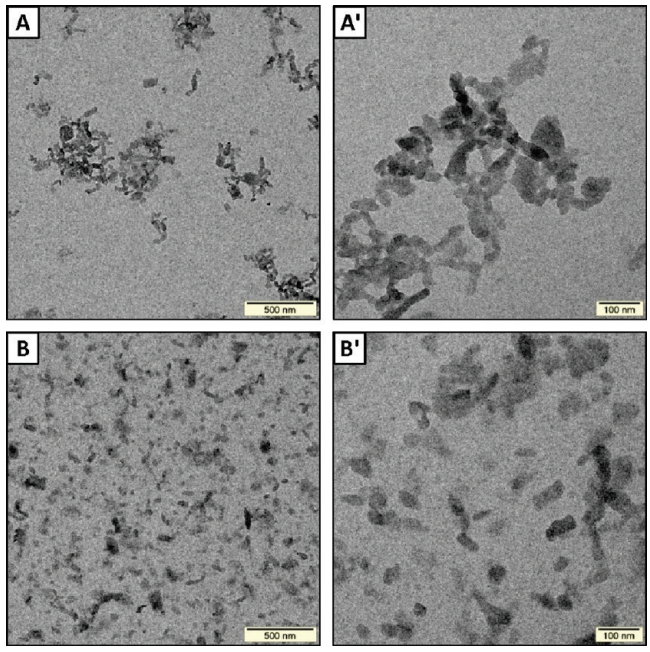

FIGURE 5. Transmission electron microscopy images of PY-185 nanoparticles coated on ultrathin amorphous carbon film. Without synergist presence: (A) large area view (2.5 × 2.5 μm^2) and (A′) a 0.8 × 0.8 μm^2 zoom view of A. With synergist: (B) imaged with a scan size of 2.5 × 2.5 μm^2 and (B′) a zoom view (0.8 × 0.8 μm^2) of B.

the reference dispersion and the dispersion incorporating the synergist. Transmission electron microscopy images of PY-185 nanoparticles coated on ultrathin amorphous carbon film are shown in Figure 5. The nanoparticles have platelet morphology with an estimated thickness in the 10−20 nm range. The longest dimension observed for the platelets ranged from less than 20 to 100 nm. A significant if not a dominant number of platelets observed are less than 50 nm in size based on the longest dimension. The images clearly show that the nanoparticle platelets that were dispersed in the presence of the synergist (Figure 5B) are less aggregated. In addition, no significant difference in particle size was detected between the reference and synergist dispersed nanoparticles. This supports the position that the DLS bimodal plot of the reference dispersion was the result of significant nanoparticle aggregation.

To determine if the improved yellow dispersion formulation containing the synergist translated into improved optical properties of thin-films, we coated the preceding dispersions on glass plates and characterized them by atomic force microscopy and total transmittance spectrophotometry. Analysis with AFM was used to evaluate the uniformity of the coatings of pigment nanoparticles.

In the topography AFM image shown in Figure 6A, approximately eight bright zones of dense nanoparticle aggregates are apparent within the 20 × 20 μm^2 scan, covering 8% of the total surface. The lateral dimensions of these taller domains ranged from 500 to 2000 nm, and the average height measured 200 nm. A zoom-in view of the central region without the dense clusters is displayed in Figure 6A′. The image exhibits a tightly packed arrangement of pigment nanoparticles on the surface; the overall dimensions of the dense areas ranges from 100 to 270 nm. The rms roughness measured 9.1 nm for the area displayed in Figure 6A′. The simultaneously acquired phase image in Figure 6A″ reveals a uniform color for the nanoparticles. The homogeneous color suggests a highly consistent surface composition without evidence of contamination or additives. The corresponding cursor profile of Figure 6A‴ measured 50 nm, whereas the cluster had a height of approximately 150 nm.

Similar to the coating prepared from the reference dispersion, the synergist-containing coating was also characterized using tapping mode AFM. The images are shown in the bottom panels of Figure 6. A few small areas of dense nanoparticle clusters are still present in the wide area topography view of Figure 6B; however, the areas are considerably smaller in dimension. The overall regions of dense aggregates cover approximately 1.5% of the surface, and lateral dimensions of the dense areas range from 60 to 80 nm. The heights of the bright zones measure 120 ± 26 nm, referencing the shallowest area of the surface as a baseline. A close-up view (Figure 6B′) more clearly displays the morphology of pigment aggregates, which range from 50 to 150 nm in size. The rms roughness for the 2.5 × 2.5 μm^2 frame measures 7.9 nm. The corresponding phase image in Figure 6B″ exhibits interesting surface changes that are not apparent in the topography frames. Two distinct colors are evident; the dark areas identify the synergist material added to the dispersion. The sample contains a well-dispersed molecular adsorbate mixed with the pigment nanoparticles, in contrast to the reference sample image shown in Figure 6A. Phase images provide a highly sensitive map for distinguishing differences in the chemical composition of surfaces. The phase data clearly displays the intercalation of the synergist located at edges surrounding nanoparticles throughout the sample. The line profile presented in Figure 6B‴ shows a pigment nanoparticle cluster with a height of approximately 120 nm.

The influence of the synergist is indicated by smaller aggregates in coatings prepared from synergist-containing dispersions relative to coatings prepared from the reference dispersion. This is supported by the cursor profile of the synergist coating represented in Figure 6B‴ showing fewer and shorter clusters compared to the reference coating. In addition, the surface coverage for areas of high density for

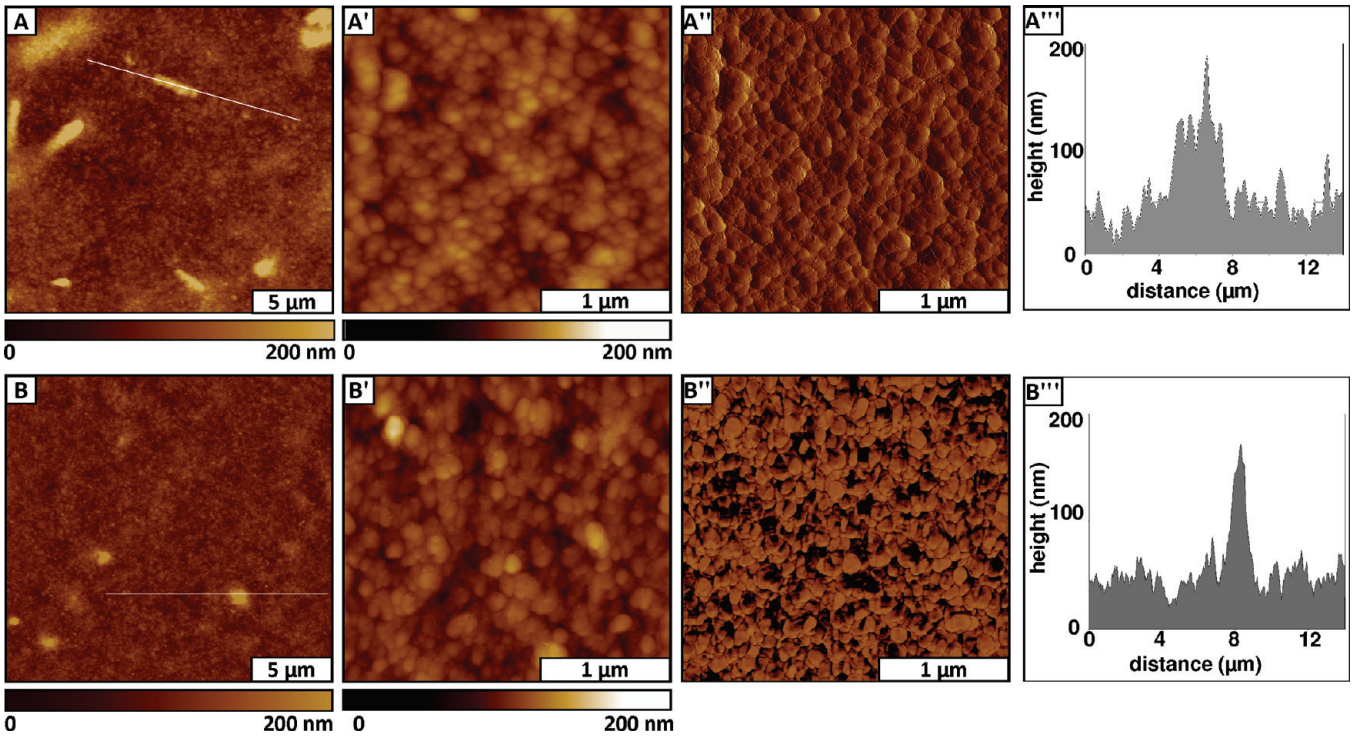

FIGURE 6. Surface views of coated pigment nanoparticles prepared with polymeric dispersant only: (A) Tapping mode AFM topography image (20 × 20 μm^2); (A′) zoom-in topograph (2.5 × 2.5 μm^2); (A″) phase image for A′; (A‴) cursor profile of A. Images of coated pigment nanoparticles prepared with polymeric dispersant in the presence of a synergist: (B) Wide area topograph (20 × 20 μm^2); (B′) zoom-in view of B (2.5 × 2.5 μm^2); (B″) phase image for B′; (B‴) profile for the line in B.

the synergist coating was reduced from 8.6 to 1.5%. The rms roughness of the surface was shown to decrease slightly from 9.1 to 7.0 nm for coatings containing the synergist. The values of rms roughness were calculated for local areas of the surface, and are not necessarily an indicator of surface changes for the entire sample. The values of rms roughness change considerably from frame to frame, even for the same sample. It should be noted the convolution of tip geometry could affect roughness measurements, as well as the size of the area selected for measurements. Therefore, the rms roughness provides a relative indicator of local changes only for selected areas of the same dimensions, which are representative of areas viewed throughout the surface. The rms roughness can be helpful for local comparisons with AFM, but is not a definitive estimate of macroscopic roughness.

Research on pigment nanoparticles has shown the least aggregated or more dispersed pigment nanoparticles normally leads to sharper spectral features and hence transmits more light (5, 19). To confirm that reduction in nanoparticle aggregates of the coated dispersions translates into improved optical properties, each coating was characterized by total transmittance spectrophotometry. A comparison of the total transmittance spectra in the visible wavelength region for the coated dispersions is presented in Figure 7. Figure 7B displays a zoom-in on the 490−727 nm wavelength region to show that the least aggregated coating prepared from the synergist-containing yellow dispersion has the sharpest-cutting total spectral transmittance features.

To determine the solvent influence on dispersion properties, synergist-containing dispersions of PY-185 were prepared using solvent mixtures. The standard solvent PGMEA was combined in different ratios with cyclohexanone. Dispersions were prepared using 3:1 and 1:1 ratios of PGMEA and cyclohexanone, respectively. Size analyses of resulting

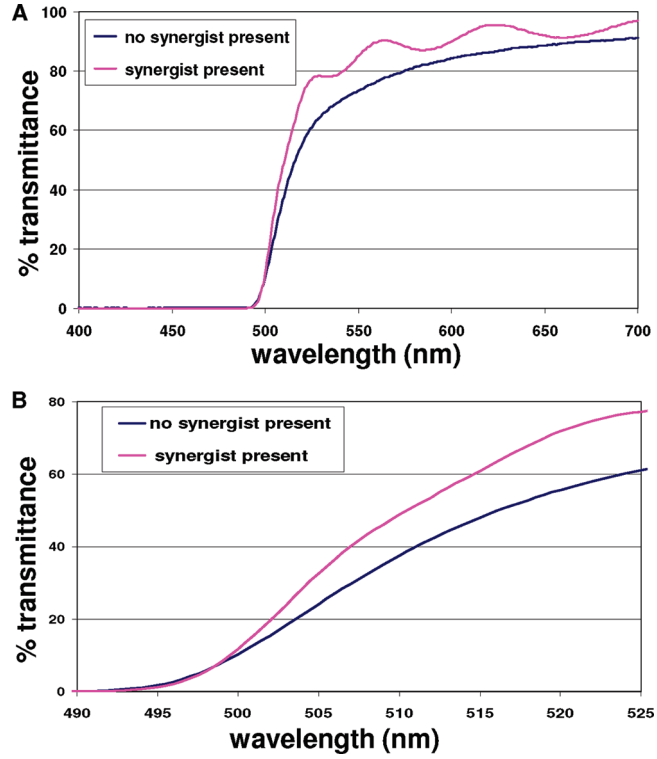

FIGURE 7. Transmittance spectra of coated dispersions with and without synergist present: (A) visible wavelength region; (B) zoom-in view of 490−525 nm.

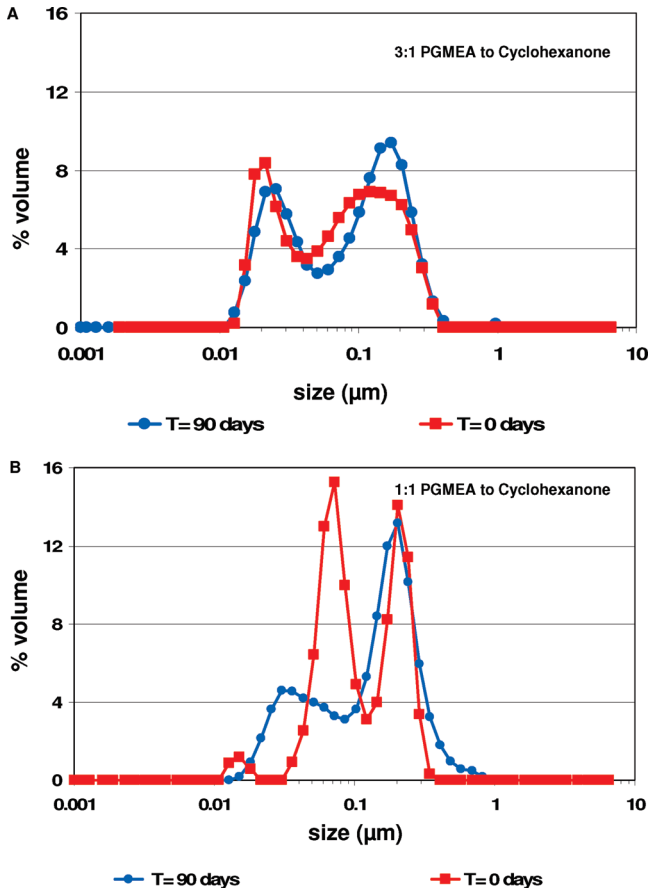

FIGURE 8. Size distribution of pigment nanoparticles prepared with a synergist dispersed in mixtures of PGMEA and cyclohexanone. (A) Data acquired directly after dispersion were prepared with a 3:1 PGMEA/cyclohexanone ratio and after aging for 90 days. (B) Data acquired directly after dispersion was prepared with a 1:1 PGMEA/cyclohexanone ratio and after aging for 90 days.

dispersions were obtained from DLS measurements for the mixed solvent dispersions (Figure 8). For the dispersion prepared using a solvent ratio of 3:1, analysis immediately after preparation showed 38% of the nanoparticles ranged from 10 to 43 nm in size and 63% ranged from 43 to 350 nm. After aging, measurements showed a slight shift toward larger sizes. However, overall 36% of the nanoparticles still were within the 10 to 43 nm range. The shape of the second peak became sharper, showing a particle size range of 43 to 980 nm. (Figure 8B). Results were similar for the dispersion prepared with a 1:1 mixture of PGMEA to cyclohexanone (Figure 8A). Three peaks were apparent, showing 3% of the nanoparticles are less than 20 nm in size, 56% ranged from 20 to 125 nm, and 41% covered the size range of 125 to 350 nm. After 90 days, the particle size distribution changed more significantly, showing a greater percentage of larger particles. The DLS distribution showed 43% in the 10 to 125 nm range and 58% ranged from 125 nm to as large as 820 nm. On the basis of the larger particle size distributions, the presence of cyclohexanone apparently results in increased nanoparticle aggregation. It is possible that shifting to a higher dielectric solvent ($\varepsilon = 18.2$ for cyclohexanone versus 8.3 for PGMEA) disrupts the proposed stabilizing ion-pair interactions. Cyclohexanone also promotes dispersion instability.

Samples of the mixed-solvent dispersions were also spin-coated on glass and imaged with tapping-mode AFM to determine the nanoscale morphology. The coatings from dispersions prepared with a 3:1 ratio of PGMEA to cyclohexanone are shown in the upper panels of Figure 9. The lower panels of Figure 9 show coatings prepared from the 1:1 solvent mixture. Multiple areas were examined throughout the sample, and the results of Figure 9 are representative of the morphologies of the entire surface. Comparing the upper versus lower topography frames for the different solvent mixtures, the samples are mostly indistinguishable. Even for the $2.5 \times 2.5\ \mu m^2$ zoom-in view, the shapes and arrangements of pigment nanoparticles within the films are quite similar for Figure 9A′ (3:1 ratio PGMEA:cyclohexanone) as compared to Figure 9B′ (1:1 ratio PGMEA:cyclohexanone). As a quantitative estimate, the rms value for Figure 9A′ measured 13 nm compared to 15 nm for Figure 9B′, which further indicates that the surface morphologies are quite similar for the two samples. Because of extensive aggregation, nanoparticle clusters could not be observed from the mixed solvent coatings. There are two colors apparent within the phase images; there is a dark outline within the grooves and spaces between pigment nanoparticles in A″ and B″ in Figure 9, which corresponds to areas with intercalated synergist, as shown previously for the phase image of Figure 6B. An estimate of the surface area of the regions containing synergist measured $45 \pm 5\%$ and $43 \pm 5\%$ for A″ and B″ in Figure 9, respectively.

Surface analysis by AFM also indicates the large clusters viewed in solution by DLS do not necessarily persist when the samples are spin-coated on surfaces; the forces of surface adhesion can often break the clusters into smaller assemblies when films are formed under centrifugal force. The sizes of nanoparticle aggregates within surface films are often quite different than sizes of clusters dispersed in solutions; therefore, when comparing DLS results to AFM measurements, the results often show differences for size measurements.

Changing the polarity of the dispersion solvent was shown to be quite effective for preventing dense zones of pigment nanoparticles from forming within spin-coated films. Whether the solvent composition was composed of predominantly PGMEA or equal parts with cyclohexanone, the surface topologies were indistinguishable for samples prepared. Surface chemistry was unchanged as viewed with phase images, and the rms roughness was quite similar for samples prepared with the two different solvent ratios.

A comparison of the total transmittance spectral plots of coatings prepared from the mixed solvent dispersions is shown in Figure 10. Included in the comparison are the reference nonsynergist and the PGMEA only with synergist coatings. Relative to the reference nonsynergist coating, a trend of increased transmittance was observed for coatings that contained the synergist. Coatings from mixed-solvent dispersions with synergist have total spectral transmittance properties that fall in the middle of the reference (without

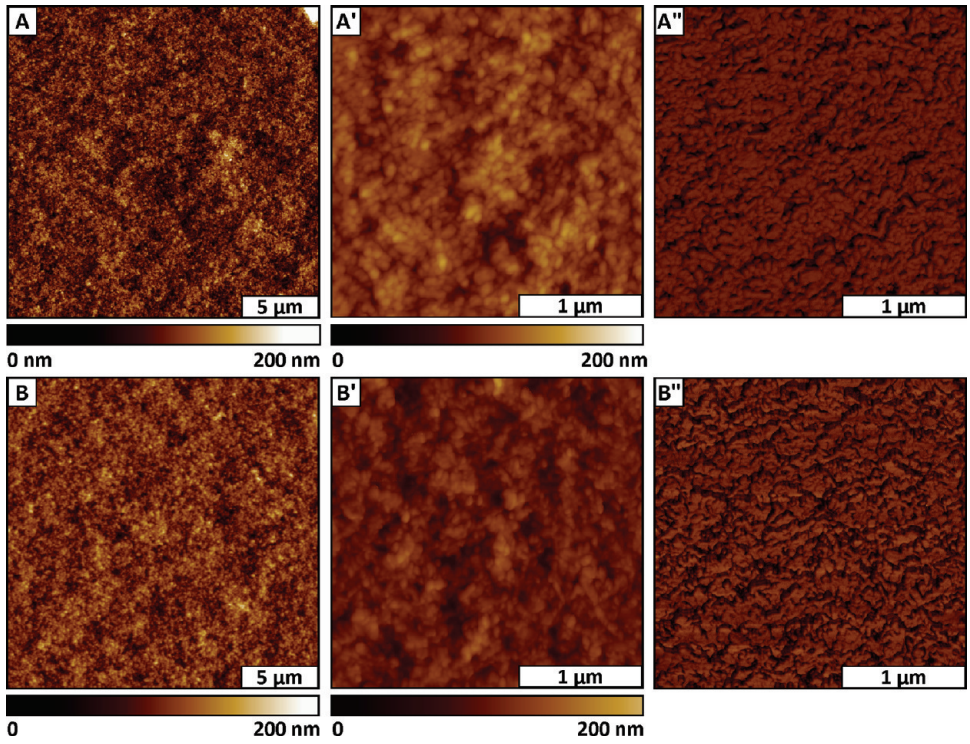

FIGURE 9. Surface views of pigment nanoparticles coated from 3:1 PGMEA/ cyclohexanone ratio. (A) Wide view AFM topograph (20 × 20 μm^2); (A′) zoom-in view (2.5 × 2.5 μm^2); (A″) corresponding phase channel for A′. Images of pigment nanoparticles coated from 1:1 PGMEA/ cyclohexanone ratio: (B) AFM topograph (20 × 20 μm^2); (B′) zoom-in view (2.5 × 2.5 μm^2); (B″) phase image for B′. Both dispersion mixtures contain synergist.

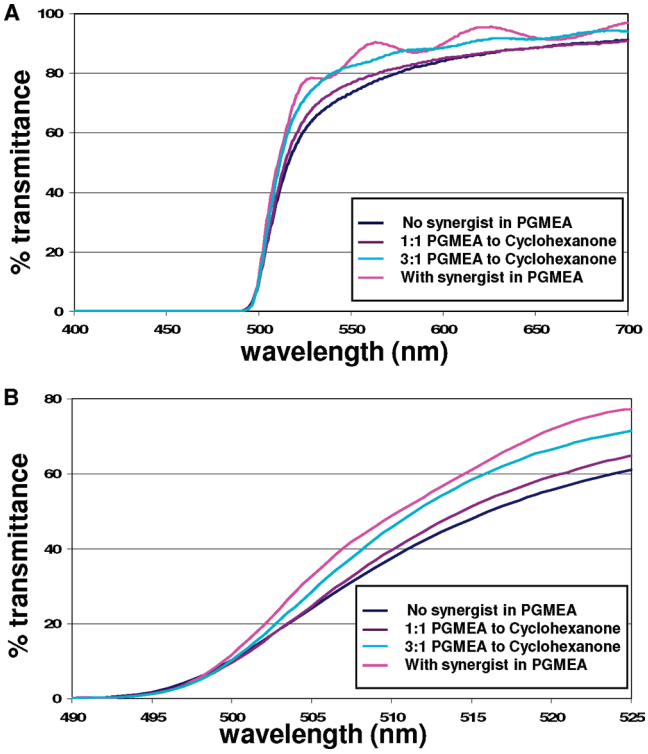

FIGURE 10. Transmittance spectra of coated dispersions showing influence of synergist and solvent systems.

synergist) and the pure PGMEA with synergist coatings. Although AFM images did not distinguish a difference in the degree of nanoparticle aggregation for the mixed-solvent coatings, the coating from the 3:1 solvent mixture was sharper cutting in its total spectral transmittance properties than the coating from the dispersion with the 1:1 solvent ratio.

The results would be consistent with increased aggregation as the solvent shifts to higher polarity. These spectral studies show the impact of nanoparticle aggregation on the ability to obtain desirable sharp-cutting spectral characteristics and increased transmitted light for thin films prepared from pigment nanoparticles.

CONCLUSIONS

An acid-functionalized synergist can be used for enhancing the interaction between an amine functionalized polymeric dispersant and PY-185 which also incorporated amine functionality. Data supports the formation of strong ion pair interactions with the synergist that link the dispersant to the surface of generated nanoparticles. Specifically, with supporting data from DLS, TEM and AFM analyses, it was determined that the presence of the acid functionalized synergist reduced nanoparticle aggregation. Data also indicated that solvent polarity possibly plays a role in nanoparticle aggregation. This study produced a very low viscosity dispersion consisting of uniformly dispersed PY-185 nanoparticles less than 50 nm in size. These properties were observed with a pigment concentration that measured close to 10 wt %. Total transmission spectroscopy studies showed advancement of dispersion properties could be leveraged to provide improved optical properties of coated films composed of pigment nanoparticles. The investigation provides insight on how to advance the performance of optical thin films that incorporate pigment nanoparticles. This work also

identifies key dispersion properties that can be exploited and used as a guide for future studies.

Acknowledgment. The authors gratefully acknowledge support from the State of Louisiana Board of Regents, research competitiveness subprogram (LEQSF(2006-09)-RD-A-04), and the National Science Foundation Career program (CHE-0847291). A.T.K. thanks Eastman Kodak for sponsoring a research internship during 2008 and Kenneth Johnson, John Bryant, and Essie Calhoun for their support.

Supporting Information Available: Further tapping mode-AFM images of pigment dispersion spin-coating (PDF). This material is available free of charge via the Internet at http://pubs.acs.org

REFERENCES AND NOTES

(1) Bilgili, E.; Hamey, R.; Scarlett, B. *Chem. Eng. Sci.* **2006**, *61*, 149–157.
(2) Horn, D.; Rieger, J. *Angew. Chem., Int. Ed.* **2001**, *40* (23), 4331–4361.
(3) Mendel, J.; Bugner, D.; Bermel, A. D. *J. Nanopart. Res.* **1999**, *1* (3), 421–424.
(4) Zheng, T. H.; Choy, W. C. H.; Sun, Y. X. *Appl. Phys. Lett.* **2009**, *94* (12), 3.
(5) Carotenuto, G.; Her, Y. S.; Matijevic, E. *Ind. Eng. Chem. Res.* **1996**, *35* (9), 2929–2932.
(6) Qu, D.; Duncan, J. W. *J. Cosmet. Sci.* **2000**, *51*, 323–341.
(7) Baez, E.; Quazi, N.; Ivanov, I.; Bhattacharya, S. N. *Adv. Powder Technol.* **2009**, *20* (3), 267–272.
(8) Fu, S. H.; Fang, K. J. *J. Dispersion Sci. Technol.* **2006**, *27* (7), 971–974.
(9) Hao, Z. M.; Iqbal, A. *Chem. Soc. Rev.* **1997**, *26* (3), 203–213.
(10) Haq, I.; Fraser, I.; Matijevic, E. *Colloid Polym. Sci.* **2003**, *281* (6), 542–549.
(11) Hong, L.; Guo, J.; Gao, Y.; Yuan, W.-K. *Ind. Eng. Chem. Res.* **2000**, *39* (12), 4882–4887.
(12) Ishibashi, M.; Hotta, Y.; Ushirogochi, T.; Akiyama, R.; Kawakami, Y.; Ohtsu, K.; Kiyomoto, H.; Tanuma, C. *J. Photopolym. Sci. Technol.* **2006**, *19* (5), 653–656.
(13) Mukhopadhyay, P.; Desbaumes, L.; Schreiber, H. P.; Hor, A. M.; DipaolaBaranyi, G. *J. Appl. Polym. Sci.* **1998**, *67* (2), 245–253.
(14) Van, S. T.; Velamakanni, B. V.; Adkins, R. R. *J. Coat. Technol.* **2001**, *73*, 61–70.
(15) Widiyandari, H.; Iskandar, F.; Hagura, N.; Okuyarna, K. *J. Appl. Polym. Sci.* **2008**, *108* (2), 1288–1297.
(16) Grubenmann, A. *Part. Part. Syst. Charact.* **1986**, *3* (4), 179–186.
(17) Spinelli, H. J. *Adv. Mater.* **1998**, *10* (15), 1215–218.
(18) Maikowski, M. *Prog. Colloid Polym. Sci.* **1976**, *59*, 70–81.
(19) Cheng, W. T.; Hsu, C. W.; Chih, Y. W. *J. Colloid Interface Sci.* **2004**, *270* (1), 106–112.
(20) Bilgili, E.; Hamey, R.; Scarlett, B. *China Particuology* **2004**, *2* (3), 93–100.
(21) Chang, C. J.; Chang, S. J.; Tsou, S.; Chen, S. I.; Wu, F. M.; Hsu, M. W. *J. Polym. Sci., Part B: Polym. Phys.* **2003**, *41* (16), 1909–1920.
(22) Schoff, C. K. *Prog. Org. Coat.* **2005**, *52*, 21–27.
(23) Schofield, J. D. *Prog. Org. Coat.* **2002**, *45* (2−3), 249–257.
(24) Tsubokawa, N.; Kobayashi, M.; Ogasawara, T. *Prog. Org. Coat.* **1999**, *36* (1−2), 39–44.
(25) Zhang, T. Y.; Fei, X. N.; Wang, S. R.; Zhou, C. L. *Dyes Pigm.* **2000**, *45* (1), 15–21.
(26) Subra, P.; Jestin, P. *Powder Technol.* **1999**, *103* (1), 2–9.
(27) Hayashi, K.; Morii, H.; Iwasaki, K.; Horie, S.; Horiishi, N.; Ichimura, K. *J. Mater. Chem.* **2007**, *17* (6), 527–530.
(28) Horiuchi, S.; Horie, S.; Ichimura, K. *ACS Appl. Mater. Interfaces* **2009**, *1* (5), 977–981.
(29) Park, J. W.; Ullah, M. H.; Park, S. S.; Ha, C. S. *J. Mater. Sci.: Mater. Electron.* **2007**, *18*, S393–S397.
(30) Sun, C. J.; Wu, Y.; Xu, Z. H.; Hu, B.; Bai, J. M.; Wang, J. P.; Shen, J. *Appl. Phys. Lett.* **2007**, *90* (23), 3.
(31) Mayer, T.; Weiler, U.; Kelting, C.; Schlettwein, D.; Makarov, S.; Wöhrle, D.; Abdallah, O.; Kunst, M.; Jaegermann, W. *Sol. Energy Mater. Sol. Cells* **2007**, *91* (20), 1873–1886.
(32) Deroover, G. Patent Application U.S. 200894451A, 2008.

AM9005836